Hexagonal warping on optical conductivity of surface states in Topological Insulator Bi_2Te_3

Zhou Li^{1*} and J. P. Carbotte^{1,2}

Department of Physics, McMaster University, Hamilton, Ontario, Canada,L8S 4M1
 Canadian Institute for Advanced Research, Toronto, Ontario, Canada M5G 1Z8
 (Dated: November 9, 2018)

ARPES studies of the protected surface states in the Topological Insulator Bi_2Te_3 have revealed the existence of an important hexagonal warping term in its electronic band structure. This term distorts the shape of the Dirac cone from a circle at low energies to a snowflake shape at higher energies. We show that this implies important modifications of the interband optical transitions which no longer provide a constant universal background as seen in graphene. Rather the conductivity shows a quasilinear increase with a slightly concave upward bending as energy is increased. Its slope increases with increasing magnitude of the hexagonal distortion as does the magnitude of the jump at the interband onset. The energy dependence of the density of states is also modified and deviates downward from linear with increasing energy.

PACS numbers: 72.20.-i, 75.70.Tj, 78.67.-n

I. INTRODUCTION

Topological Insulators are insulating in the bulk and have symmetry protected helical Dirac fermions on their surface with an odd number of Dirac points in the surface state Brillouin zone. 1-9 The surface charge carriers are massless and relativistic with linear in momentum energy dispersion curves. Spin sensitive angular resolved photo emission spectroscopy (ARPES) also shows that their spins are locked to their momentum. The position of the chemical potential relative to the Dirac point and the gapped bulk bands is not as easily tuned as it is in graphene¹⁰ but can be controlled by doping with Sn in $(Bi_{1-\delta}Sn_{\delta})_2Te_3$ or with Ca in $Bi_{2-\delta}Ca_{\delta}Te_3$ with further dosing with NO_2 molecules. The constant energy contours in Bi_2Te_3 as measured by ARPES are not circles as they are in graphene but have an hexagonal distortion which gives them snowflake shape. This geometry was modeled by Fu¹¹ with an unconventional hexagonal warping term in the bare band Hamiltonian of Bi_2Te_3 with parameters fit to the measured Fermi surface.

Optical spectroscopy has been a very powerful method to obtain valuable information on the charge dynamics of the Dirac fermions in graphene. $^{12-14}$ An experimental review was given by Orlita and Potemski. 15 Usually it is the zero momentum q limit of the optical conductivity as a function of photon energy which is measured but very recently finite q's have also been measured using near field techniques. $^{16-19}$ Optics has also been used to study topological insulators. $^{20-22}$ In this paper we study how hexagonal warping in Bi_2Te_3 manifest in the optical conductivity, which we find is profoundly modified for the parameters determined in the work of Fu. 11

II. FORMALISM

The Hamiltonian used by Fu¹¹ to describe the surface states band structure near the Γ point in the surface Bril-

louin zone is

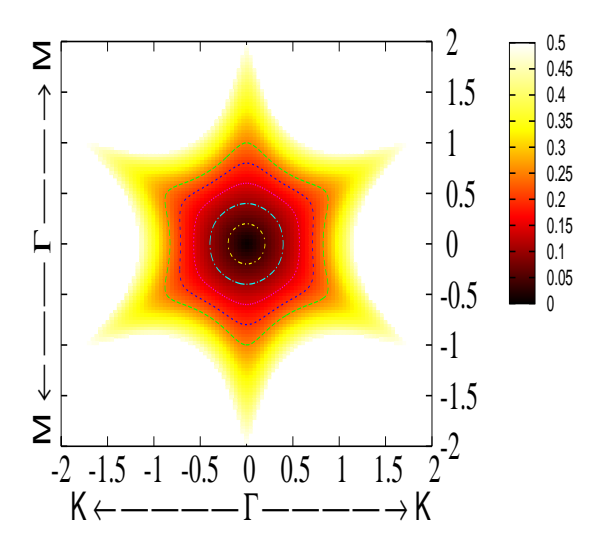
$$H_0 = v_k (k_x \sigma_y - k_y \sigma_x) + \frac{\lambda}{2} (k_+^3 + k_-^3) \sigma_z + E_0(k) \quad (1)$$

where $E_0(k) = \hbar^2 k^2/(2m^*)$ is a quadratic term which gives the Dirac fermionic dispersion curves an hour glass shape and provides particle-hole asymmetry. The Dirac fermion velocity to second order is $v_k = v_F (1 + \alpha k^2)$ with v_F the usual Fermi velocity measured to be $2.55eV \cdot \mathring{A}$ and α is a constant which is fit along with m^* to the measured band structure in the reference [11]. The hexagonal warping parameter $\lambda = 250eV \cdot \mathring{A}^3$. The σ_x , σ_y , σ_z are the Pauli matrices here referring to spin, while in graphene these would relate to pseudospin instead. Finally $k_{\pm} = k_x \pm i k_y$ with k_x , k_y momentum along x and y axis respectively. The energy spectrum associated with the Hamiltonian [Eq. (1)] is

$$E_{\pm}(k) = E_0(k) \pm \sqrt{v_k^2 k^2 + \lambda^2 k^6 \cos^2(3\theta)}$$
 (2)

where θ is the polar angle defining the direction of k in the two dimensional surface state Brillouin zone. The energy dispersion curves in Eq. (2) reduce to the well known linear law $\pm v_k k$ of graphene when E_0 is set zero along with $\lambda=0$, i.e. ignoring hexagonal warping. Since our primary interest here is getting a first understanding of how the warping term in Eq. (2) manifests itself in the dynamical conductivity of the surface helical Dirac fermions we will for simplicity from here on drop the $E_0(k)$ term which as we have said provides particle-hole asymmetry.

In FIG. 1 we show a color plot for the constant energy contour associated with the dispersion curves [Eq. (2)] as the energy is increased above that of the Dirac point the contour changes shape and shows greater hexagonal distortion displaying a snowflake shape. The largest flake shown corresponds to a chemical potential of 250meV which is achieved when $\delta = 0.67\%$ in $(Bi_{1-\delta}Sn_{\delta})_2Te_3$. In graphene we would have circles for all energies and



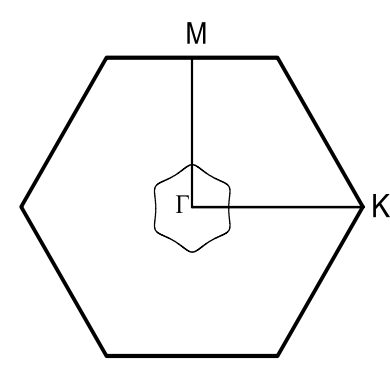


FIG. 1. (Color online) Constant energy contours for the dispersion curves used to describe the bare bands in Bi_2Te_3 with chemical potential μ changed by doping with Sn in $(Bi_{1-\delta}Sn_{\delta})_2Te_3$ where $\delta=.67\%$ corresponds to a chemical potential $\mu=250meV$. The kx and ky axes are in the units of $0.1\mathring{A}^{-1}$. Also shown is the surface state Brillouin zone identifying Γ, K and M points.

in strained graphene we would have elliptical contours instead of circle.

The Kubo formula for the xx component of the dynamic conductivity $\sigma_{xx}(\omega)$ as a function of photon energy ω is given in terms of the matrix Matsubara Green's function $\hat{G}(k,\omega_n)$ with ω_n the Fermionic Matsubara imaginary frequency as

$$\sigma_{xx}(\omega) = -\frac{e^2}{i\omega} \frac{1}{4\pi^2} \int_0^{k_{cut}} k dk d\theta$$

$$T \sum_l Tr \langle v_x \hat{G}(\mathbf{k}, \omega_l) v_x \hat{G}(\mathbf{k}, \omega_n + \omega_l) \rangle_{i\omega_n \to \omega + i\delta}$$
 (3)

with e the charge on the electron, k the absolute value of the momentum with direction θ and k_{cut} a cut off. Here T is the temperature with $\omega_n = (2n+1)\pi T$ and $\omega_l = 2l\pi T$ the Fermion and Boson Matsubara frequencies, 23 n and

l are integers and Tr is a trace. To get the conductivity which is a real frequency quantity, we needed to make an analytic continuation from imaginary $i\omega_n$ to real ω and δ is infinitesimal. As written we have neglected vertex correction and so the factors v_x are simply the velocity components given by

$$v_x = v_k \sigma_y + 3\lambda k^2 \cos(2\theta) \sigma_z \tag{4}$$

$$v_y = -v_k \sigma_x - 3\lambda k^2 \sin(2\theta)\sigma_z \tag{5}$$

obtained directly from the Hamiltonian [Eq. (1)]. We have set all \hbar factors equal to one.

The matrix Green's function for the non-interacting bare band is given by

$$\frac{\hat{G}_{0}(\mathbf{k}, i\omega_{n})}{i\omega_{n} + \mu - v_{k}(k_{x}\sigma_{y} - k_{y}\sigma_{x}) - \frac{\lambda}{2}(k_{+}^{3} + k_{-}^{3})\sigma_{z}}
= \frac{i\omega_{n} + \mu + v_{k}(k_{x}\sigma_{y} - k_{y}\sigma_{x}) + \lambda k^{3}\cos(3\theta)\sigma_{z}}{(i\omega_{n} + \mu)^{2} - v_{x}^{2}k^{2} - \lambda^{2}k^{6}\cos^{2}(3\theta)}$$
(6)

with

$$(k_{+}^{3} + k_{-}^{3})^{2} = (2k_{x}^{3} - 6k_{x}k_{y}^{2})^{2} = 4k^{6}\cos^{2}(3\theta)$$
 (7)

It is convenient to rewrite the $\hat{G}_0(\mathbf{k}, i\omega_n)$ in terms of $\hat{G}_0(\mathbf{k}, s, i\omega_n)$ defined as

$$G_0(\mathbf{k}, s, i\omega_n) = \frac{1}{i\omega_n + \mu - s\sqrt{v_k^2 k^2 + \lambda^2 k^6 \cos^2(3\theta)}}$$
(8)

where $s = \pm 1$ and \mathbf{F}_k defined as

$$\mathbf{F}_k = \frac{(-v_k k \sin \theta, v_k k \cos \theta, \lambda k^3 \cos(3\theta))}{\sqrt{v_k^2 k^2 + \lambda^2 k^6 \cos^2(3\theta)}}$$
(9)

This gives

$$\hat{G}_0(\mathbf{k}, i\omega_n) = \frac{1}{2} \sum_{s=\pm} (1 + s\mathbf{F}_k \cdot \sigma) G_0(\mathbf{k}, s, i\omega_n)$$
 (10)

III. SIMPLIFICATION OF EXPRESSION FOR $\sigma_{xx}(\omega)$

We will be interested here only with the interband terms in which case the required trace gives

$$Tr\langle v_x \hat{G}(\mathbf{k}, \omega_l) v_x \hat{G}(\mathbf{k}, \omega_l + \omega_n) \rangle$$

$$= \frac{H(\theta)}{[v_k^2 k^2 + \lambda^2 k^6 \cos^2(3\theta)]}$$

$$(\frac{1}{i\omega_n + \mu - E_-} \frac{1}{i\omega_n + i\omega_l + \mu - E_+}$$

$$+ \frac{1}{i\omega_n + \mu - E_+} \frac{1}{i\omega_n + i\omega_l + \mu - E_-})$$
(11)

where

$$H(\theta) = \lambda^2 v_k^2 k^6 [\cos^2(3\theta) - 3\cos\theta\cos(2\theta)\cos(3\theta) + 9\cos^2(2\theta)] + v_k^4 k^2 \sin^2\theta$$
(12)

But we know that

$$T \sum_{l} \left[\frac{1}{i\omega_{l} + \mu - E_{-}} \frac{1}{i\omega_{l} + i\omega_{n} + \mu - E_{+}} + \frac{1}{i\omega_{l} + \mu - E_{+}} \frac{1}{i\omega_{l} + \mu - E_{+}} \right]$$

$$= \left[\frac{f(E_{-}) - f(E_{+})}{i\omega_{n} - E_{+} + E_{-}} + \frac{f(E_{+}) - f(E_{-})}{i\omega_{n} - E_{-} + E_{+}} \right]$$
(13)

and hence we obtain

$$\sigma_{xx}(\omega) = -\frac{e^2}{i\omega} \frac{1}{4\pi^2} \int_0^{k_{cut}} k dk d\theta \frac{H(\theta)}{[v_k^2 k^2 + \lambda^2 k^6 \cos^2(3\theta)]} \left[\frac{f(E_-) - f(E_+)}{i\omega_n - E_+ + E_-} + \frac{f(E_+) - f(E_-)}{i\omega_n - E_- + E_+} \right]_{i\omega_n \to \omega + i\delta}$$
(14)

Here f(x) is the Fermi-Dirac distribution function given by $f(x) = 1/[\exp(x/T - \mu/T) + 1]$, where we have ignored the Boltzman constant k_B but will include it in the calculation. We have verified that $\sigma_{yy}(\omega) = \sigma_{xx}(\omega)$, after an analytic continuation from imaginary to real Matsubara frequencies we obtain the final expression

$$\sigma_{xx}(\omega) = -\frac{e^2}{i\omega} \frac{1}{4\pi^2} \int_0^{k_{cut}} k dk d\theta \frac{H(\theta)}{W(k,\theta)} \times \left[\frac{f(E_-) - f(E_+)}{\omega - 2\sqrt{W(k,\theta)} + i\delta} + \frac{f(E_+) - f(E_-)}{\omega + 2\sqrt{W(k,\theta)} + i\delta} \right]$$
(15)

where $W(k, \theta) = v_k^2 k^2 + \lambda^2 k^6 \cos^2(3\theta)$.

IV. ANALYTIC FORM FOR THE REAL PART OF CONDUCTIVITY

The real part of the dynamic conductivity which is the absorptive part can be simplified further using the usual rule $\frac{1}{\omega + i\delta} = \frac{P}{\omega} - i\pi\delta(\omega)$. From Eq. (15) we get

$$Re\sigma_{xx}(\omega) = -\frac{e^2}{\omega} \frac{1}{4\pi^2} \int_0^{k_{cut}} k dk d\theta H(\theta) \times \frac{[f(E_-) - f(E_+)]}{[W(k,\theta)]} (-\pi) \delta(\omega - 2\sqrt{W(k,\theta)})$$
(16)

which can be rewritten as

$$Re\sigma_{xx}(\omega) = \frac{e^2}{2\omega} \frac{1}{4\pi} \int_0^{k_{cut}} d(k^2) d\theta \frac{H(\theta)}{\omega^2/4} \times [f(-\omega/2) - f(\omega/2)] \delta(\omega - 2\sqrt{W(k,\theta)})$$
(17)

and we get

$$Re\sigma_{xx}(\omega) = \frac{e^2[f(-\omega/2) - f(\omega/2)]}{24\pi\omega^2} \times \int_0^{k_{cut}} \frac{d(k^2)H(\theta_{k,\omega})}{|\lambda^2 k^6 \cos(3\theta_{k,\omega})\sin\theta_{k,\omega}|}$$
(18)

where the thermal factor $f(\omega)$ have been pulled out of the integral over momentum. The Dirac delta function has been used in the process. We wrote

$$\delta(\omega - 2\sqrt{W(k,\theta)}) = \frac{\omega\delta(\theta - \theta_{k,\omega})}{|12\lambda^2 k^6 \cos(3\theta_{k,\omega})\sin\theta_{k,\omega}|}$$
(19)

where

$$\theta_{k,\omega} = \pm \frac{1}{3} \arccos\left[\pm \sqrt{\frac{\omega^2/4 - v_k^2 k^2}{\lambda^2 k^6}}\right],$$

$$\pm \frac{1}{3} \left\{\arccos\left[\pm \sqrt{\frac{\omega^2/4 - v_k^2 k^2}{\lambda^2 k^6}}\right] + \pi\right\},$$

$$\pm \frac{1}{3} \left\{\arccos\left[\pm \sqrt{\frac{\omega^2/4 - v_k^2 k^2}{\lambda^2 k^6}}\right] + 2\pi\right\}.$$
 (20)

This is our final expression for the absorptive part of the conductivity. Numerical results based on this expression are given in the next section. Before doing so however we present a similar expression for the density of states $D(\omega)$ as a function of energy which could be measured in scanning tunneling microscopy (STM). By its definition

$$D(\omega) = -\frac{1}{\pi} \sum_{\mathbf{k}} Im Tr \hat{G}(\mathbf{k}, i\omega_n - > \omega + i\delta)$$
 (21)

which can be reduced to

$$D(\omega) = -\frac{1}{\pi} \frac{1}{4\pi^2} \int_0^{k_{cut}} k dk d\theta$$

$$Im\left[\frac{1}{\omega - \sqrt{W(k,\theta)} + i\delta} + \frac{1}{\omega + \sqrt{W(k,\theta)} + i\delta}\right] (22)$$

Taking the imaginary part gives

$$D(\omega) = \frac{1}{4\pi^2} \int_0^{k_{cut}} k dk d\theta \delta(\omega - \sqrt{W(k, \theta)}) \Theta(\omega) + (\omega \to -\omega)$$
(23)

which works out to

$$D(\omega) = \frac{\omega}{12\pi^2 \lambda^2} \int_0^{k_{cut}} \frac{kdk}{|k^6 \cos(3\theta'_{k,\omega}) \sin \theta'_{k,\omega}|} \Theta(\omega) + (\omega \to -\omega)$$
(24)

where $\Theta(\omega)$ is the Heaviside step function and we have used

$$\delta(\omega - \sqrt{W(k,\theta)}) = \frac{\omega \delta(\theta - \theta'_{k,\omega})}{|3\lambda^2 k^6 \cos(3\theta'_{k,\omega}) \sin \theta'_{k,\omega}|}$$
(25)

where $\theta'_{k,\omega}$ can be obtained from Eq. (20) by replacing ω with 2ω so we have $\theta'_{k,\omega} = \theta_{k,2\omega}$.

V. NUMERICAL RESULTS

In FIG. 2 we show our results for the real part of the optical conductivity $Re\sigma_{xx}(\omega)$, in units of $2\pi e^2/h$, as a function of photon energy ω for a Bi_2Te_3 doped with Sn at level $\delta=.67\%$ (see references (6) and (11)) which corresponds to a chemical potential $\mu=250meV$ and all other parameters determined in the fit by Fu.¹¹ We show four values of μ . In all cases the threshold for the start of the interband transitions is sharp and occurs at $\omega=2\mu$, as it would in graphene. The missing optical

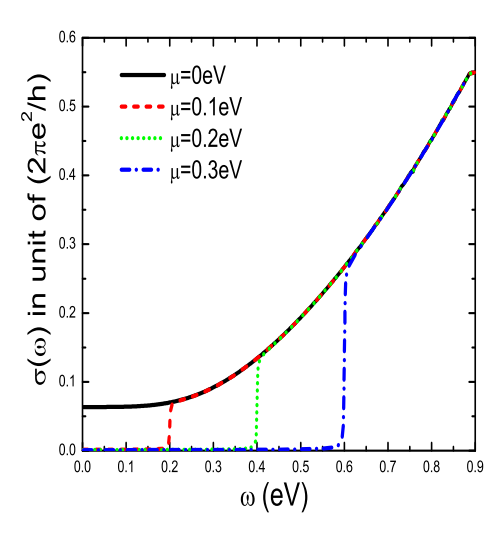


FIG. 2. (Color online) The real part of the optical conductivity $\sigma_{xx}(\omega)$ as a function of photon energy ω in meV (in units of $2\pi e^2/h$) for a case which corresponds approximately to $\delta=0.67\%$ Sn doping with chemical potential $\mu=0.25eV$. We show 4 values of μ . In all cases finite μ transfers optical spectral weight from the interband transitions to the intraband. These, not shown here, provide a Drude like contribution at ω near zero.

spectral weight in the interband transition is accompanied with an increase in the intraband (Drude) optical spectral weight. This is not shown in our picture. Because we have not included any scattering processes in our work, the Drude manifests as a Dirac delta function at $\omega = 0$ and does not overlap with the interband contribution which we emphasize here. At small values of ω , the value of $Re\sigma(\omega)$ is rather flat and takes on precisely the value expected for graphene without the degeneracy factor q = 4, which counts spin and valley degrees of freedom. For a topological insulator there is only one Dirac cone and spin is no longer degenerate. We also note that the background value is independent of material parameters such as the Fermi velocity. But this is no longer the case for a topological insulator. As ω is increased whatever the value of μ the conductivity increases rather rapidly above its universal background value and shows concave upward behavior. This is traced to the changes in fermi velocity of Eq. (4) and Eq. (5) due to the warping term proportional to λ and to the change in quasiparticle band structure. In FIG. 3 we show how $Re\sigma(\omega)$ v.s. ω is changed as λ is changed. Here and also in FIG. 4 the λ has been multiplied by the cube of the typical Fermi momentum, which is $0.1\mathring{A}^{-1}$. So $\lambda = 0.2$ here would correspond to $\lambda = 200 eV \cdot \mathring{A}^3$. For reference the case $\lambda = 0$ given as the solid black curve, corresponds precisely to graphene except for value of the degeneracy factor q. In this case the universal background, well known in the

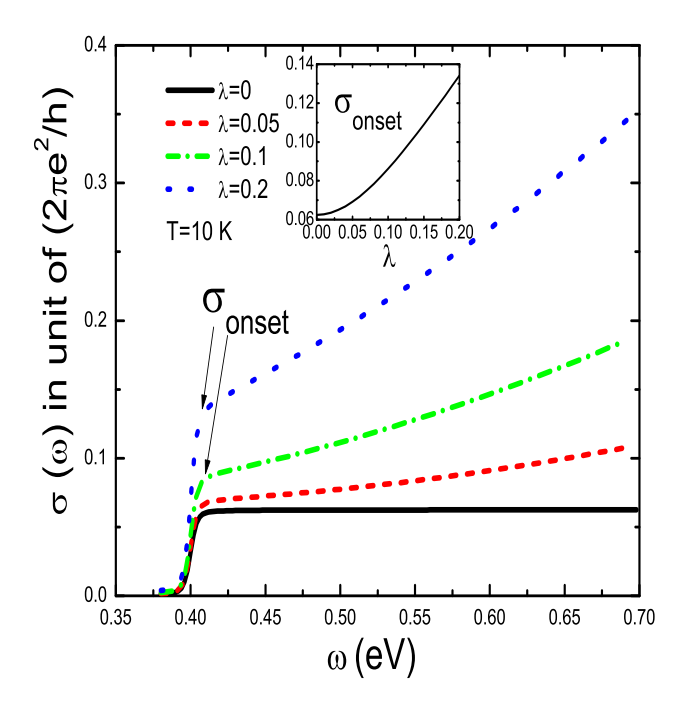


FIG. 3. (Color online) The real part of the optical conductivity $\sigma_{xx}(\omega)$ in units of $2\pi e^2/h$ as a function of photon energy for 4 values of the magnitude of the hexagonal warping term (λ) in the Hamiltonian (1). The solid black curve is for comparison. In this case $\lambda=0$ and the model reduces to the contribution to the optics of a single spin and single valley Dirac cone of graphene. In the inset we show the increase in the value of the jump at the interband absorption edge with increasing λ .

graphene literature, is recovered. As μ is increased the optical spectral weight lost in the background is transferred to the intraband contribution not shown above. Increasing λ changes the band structure and no optical sum rule applies. As λ is increased at fixed value of chemical potential μ the magnitude of the interband onset (σ_{onset}) (which remains at 2μ) increases as shown in the inset. In addition its increase at $\omega > 2\mu$ becomes even more rapid. While in the black dashed curve it is reasonably linear, the dotted curve for $\lambda = 0.2$ has acquired a significant upward curvature. These deviations from the universal background of graphene is the signature in optics of the hexagonal warping term in our Hamiltonian [Eq. (1)]. We have checked and found that these curves do not scale onto each other. The increase in $Re\sigma(\omega)$ with ω above the universal background value is to be contrasted with the behavior of the quasiparticle density of states $D(\omega)$ given by Eq. (24). As in graphene, the case $\lambda = 0$ gives $D(\omega)$ proportional to $|\omega|$. As λ is increased however $D(\omega)$ starts to deviate from linearity and, as we see in FIG. 4, is progressively reduced

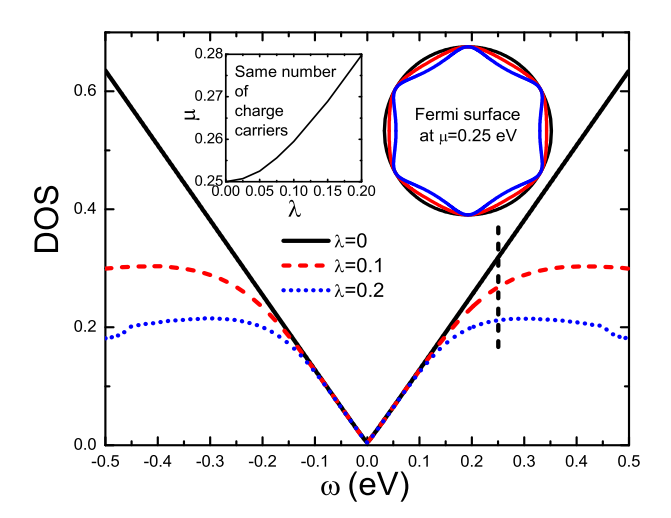


FIG. 4. (Color online) The density of state $D(\omega)$ as a function of ω . We show these for values of the hexagonal distortion term $\lambda=0$ (solid black line), $\lambda=0.1$ (dashed red line) and $\lambda=0.2$ (dotted blue line). The solid black straight line corresponds to graphene without spin and valley degeneracy. The Fermi velocity v_F was taken to be that appropriate to Bi_2Te_3 . The vertical dashed black line indicates a chemical potential $\mu=0.25eV$. The left inset gives the value of μ as a function of λ for fixed number of charge carriers which is around $1.1*10^{16}/m^2$. The right inset shows the Fermi surface at fixed value of μ for $\lambda=0$ (black), $\lambda=0.1$ (red), $\lambda=0.2$ (blue). With no hexagonal distortion it is circular and distorts to a snowflake as λ increases.

below the solid black curve. This is easily understood with the help of the right inset where we plot the constant energy contours for $\omega = \mu = 0.25 eV$ for the three value of λ considered. For $\lambda = 0$ we get the black circle of graphene theory. As λ increases this contour distorts into a snowflake pattern (blue curve) which is however completely contained inside the black circle. Of course, to keep the number of charge carriers the same we need to increase the chemical potential with increasing value of the warping parameter λ as we show in the left inset. What is plotted is the value of λ at fixed value of the number of charge carriers, which is around $1.1*10^{16}/m^2$.

VI. SUMMARY AND CONCLUSION

Helical Dirac fermions exist at the surface of a topological insulator (TI). These charge carriers have some similarity and also differences with the well known chiral Dirac fermions in graphene. An important difference is a degeneracy factor g of four which comes from the valley and spin degrees of freedom of graphene not applicable in TI. Another important difference, well investigated in the case of Bi_2Te_3 doped with Sn, is the hexagonal distortion seen in ARPES. Here we have studied how such a term changes optical properties. For realistic values of the warping parameter we found large changes in the interband transitions.

A third difference is that, graphene involves pseudospin related to the sublattice degeneracy in its two atoms per unit cell crystal structure rather than real spin. Furthermore in graphene the bands are spin degenerate, while in a topological insulator momentum and spin are locked with x-y component of real spin oriented perpendicular to its 2-D momentum k, with clockwise and anticlockwise orientation in conduction and valence band respectively.

The universal flat background observed in graphene¹³ remains at small photon energies although modified by a factor of 4 because the valley spin degeneracy no longer applies. As ω increases large modifications in the effect of the interband transitions on the conductivity are noted, and these encode the information on the hexagonal warping of the Dirac cone cross-section leading to a snowflake pattern. Instead of being flat $Re\sigma(\omega)$ increases in a quasilinear fashion with a concave upward bent. The magnitude of this linear increase becomes larger with the magnitude of the hexagonal warping term as does the value of the jump in the conductivity at the threshold of twice the chemical potential ($\omega = 2\mu$). At the same time, we find that the density of state remains linear only at small ω and starts to fall below this linear behavior at the energy where the conductivity also starts to show its deviation from a constant background value. While the conductivity curves are bent upward due to fermi velocity features, the density of state bends downward a prediction that could be verified in combined optics and scanning tunneling spectroscopy(STS) experiment.

ACKNOWLEDGMENTS

This work was supported by the Natural Sciences and Engineering Research Council of Canada (NSERC) and the Canadian Institute for Advanced Research (CIFAR).

REFERENCES

^{*} lizhou@univmail.cis.mcmaster.ca

¹ B. A. Bernevig, T.L. Hughes and S. C. Zhang, Science **314**,

- 1757 (2006).
- ² L. Fu, C. L. Kane and E. J. Mele, Phys. Rev. Lett. 98, 106803 (2007).
- ³ J. E. Moore and L. Balents, Phys. Rev. B **75**, 121306 (R) (2007).
- ⁴ J. E. Moore, Nature Phys. **5**, 378 (2009).
- ⁵ D. Hsieh et.al, Nature (London) **452**, 970 (2008).
- ⁶ Y. L. Chen et.al, Science **325**, 178 (2009).
- ⁷ D. Hsieh et.al, Science **323**, 919 (2009).
- ⁸ D. Hsieh et.al, Nature(London) **460**, 1101 (2009).
- ⁹ M. Z. Hasan and C. L. Kane, Rev. Mod. Phys. 82, 3045 (2010).
- ¹⁰ A. K. Geim and K. S. Novoselov, Nature Material 6, 183 (2007).
- ¹¹ L. Fu, Phys. Rev. Lett. **103**, 266801 (2009).
- ¹² V. P. Gusynin, S. G. Sharapov and J. P. Carbotte, Phys. Rev. Lett **98**, 157402 (2007).
- ¹³ V. P. Gusynin, S. G. Sharapov and J. P. Carbotte, New J. Phys. **11**, 095013 (2009).
- ¹⁴ Z. Li, E. A. Henriksen, Z. Jiang, Z. Hao, M. C. Martin, P. Kim, H. L. Stormer and D. N. Basov, Nat. Phys. 4, 532 (2008).
- ¹⁵ M. Orlita and M. Potemski, Semicond. Sci. Technol. **25**, 063001 (2010).
- ¹⁶ Z. Fei, G. O. Andreev, W. Bao, L. M. Zhang, A. S. McLeod, C. Wang, M. K. Stewart, Z. Zhao, G. Dominguez,

- M. Thiemens, M. M. Fogler, M. J. Tauber, A. H. Castro-Neto, C. N. Lau, F. Keilmann and D. N. Basov, Nano Lett. 11, 4701(2011).
- ¹⁷ Z. Fei, A. S. Rodin, G. O. Andreev, W. Bao, A. S. McLeod, M. Wagner, L. M. Zhang, Z. Zhao, G. Dominguez, M. Thiemens, M. M. Fogler, A. H. Castro-Neto, C. N. Lau, F. Keilmann and D. N. Basov, Nature(London). 487, 82(2012).
- J. Chen, M. Badioli, P. Alonso-González, S. Thongrattanasiri, F. Huth, J. Osmond, M. Spasenovi, A. Centeno, A. Pesquera, P. Godignon, A. Z. Elorza, N. Camara, F. J. García de Abajo, R. Hillenbrand and F. H. L. Koppens, Nature(London). 487, 77(2012).
- ¹⁹ J. P. Carbotte, J. P. F. LeBlanc and E. J. Nicol, Phys. Rev. B 85, 201411(R) (2012).
- J. N. Hancock, J. L. M. van Mechelen, A. B. Kuzmenko, D. van der Marel, C. Brüne, E. G. Novik, G. V. Astakhov, H. Buhmann, and L. W. Molenkamp, Phys. Rev. lett. 107, 136803 (2011).
- A. A. Schafgans, A. A. Taskin, Y. Ando, X. Qi, B. C. Chapler, K. W. Post, D.N. Basov, arxiv: 1202.4029 (2012).
- A. Akrap, M. Tran, A. Ubaldini, J. Teyssier, E. Giannini, D. van der Marel, P. Lerch, and C. C. Homes, Phys. Rev. B 86, 235207 (2012).
- ²³ G. D. Mahan, Many-Particle Physics, third edition, (Kluwer Academic, New York, 2000).